ChemComm

COMMUNICATION

View Article Online
View Journal | View Issue

Cite this: *Chem. Commun.*, 2019, 55, 10444

Received 4th May 2019,
Accepted 31st July 2019

DOI: 10.1039/c9cc03443a

rsc.li/chemcomm

2D metal chalcogenides with surfaces fully covered with an organic "promoter" for high-performance biomimetic catalysis†

Yanzhou Li,[ab] Jian Shu,[c] Qingqing Huang,[ab] Kashi Chiranjeevulu,[a] P. Naresh Kumar,[a] Guan-E. Wang,[a] Wei-Hua Deng,[a] Dianping Tang [c] and Gang Xu *[ab]

A new series of 2D catalytic materials whose inorganic surfaces are fully covered with pre-designed "promoter" groups are reported. One of them showed excellent biomimetic catalytic activity and provided the lowest detection limit to glucose among the reported 2D materials and their composite materials.

Nanomaterials with intrinsic enzyme mimetic activities have been intensively studied in recent years due to their advantages of easier mass preparation, higher reliability, and better chemical stability than the natural enzymes.[1–15] Among them, two-dimensional (2D) materials, such as GO–COOH, MoS_2, g-C_3N_4, WS_2, WSe_2, and Au@CuTCPP, have attracted great interest as peroxidase mimics for visual colorimetric detection of glucose due to their ultrahigh surface area, high sensitivity to external stimulants, long-term stability, *etc.*[8,16–24]

Nanozyme catalysis is a typical surface catalytic process, which is mainly determined by the number of active sites, the diffusion and adsorption of the reactant to the active sites as well as the desorption of the products from the active sites.[25] Therefore, increasing the number of active sites should be effective to optimize the catalytic properties of nanozymes. Normally, the catalytically active sites of reported 2D materials are mainly located at their edges. The methods that can increase the ratio of the edges in 2D materials, like reducing the size of 2D materials, constructing meso-structures, and cracking them into irregular morphologies have been demonstrated to be useful to increase the number of active sites.[26–30] The large specific surface of 2D materials that are expected to provide much more active sites than the edges has rarely been considered due to the difficulty in chemically functionalizing 2D materials with high density catalytically active organic functional motifs. Moreover, the surface functionalization process is normally destructive and introduces many unfavorable defects into 2D materials.

In this study, we report a series of new 2D catalytic materials, few-layered CuHBT, CuMBA and AgHBT (HBT = 4-hydroxythiophenol, MBA = 4-mercaptobenzoate), which have a thickness of only 2–3 molecular layers. The catalytic activity of this kind of surface fully functionalized 2D material was studied. Among them, the surfaces of CuHBT nanosheets are fully covered with phenol groups, which act as highly efficient "promoters" and significantly enhance the catalytic ability. This catalytic property enables CuHBT to further mimic enzymes in a cascade reaction for detecting biomolecules, such as glucose, where CuHBT showed the lowest limit of detection among all of the reported 2D materials and their composite materials.

Few-layer CuHBT was homogenously synthesized by a sonication-assisted bottom-up method. The few-layer CuMBA and AgHBT were obtained by the top-down method: (1) firstly, their bulky crystallites were prepared by the solvothermal method and (2) then, their bulky crystallites were exfoliated by a liquid exfoliation method (for details see the ESI†).[16,31–33] The structure of the parent crystal of CuHBT is presented in Fig. 1, left side, where the Cu atoms are bridged by the S atoms in HBT to form continuous $\{CuS\}_n$ inorganic layers, while the hydroxyl groups at the *para*-position of the S atoms in the ligands remain uncoordinated. As a result, $\{CuS\}_n$ layers are covered with phenol functional groups at both sides. These $\{CuS\}_n$ layers assemble with each other along the *a* axis to form the packing structure of the parent 3D structure of CuHBT. In addition, in order to investigate the active sites in CuHBT, two other ultrathin nanosheets which are isostructural to CuHBT were prepared: (1) CuMBA maintaining the $\{CuS\}_n$ layer the same but changing the functional groups from Ph–OH to Ph–COOH in the structure (Fig. 1, right side) and (2) AgHBT keeping the same Ph–OH functional groups but replacing the $\{CuS\}_n$ with the $\{AgS\}_n$ layer in the structure (Fig. 1, middle). The thickness of the monolayers of CuHBT,

[a] *State Key Laboratory of Structural Chemistry, Fujian Institute of Research on the Structure of Matter, Chinese Academy of Sciences, Fuzhou, Fujian, 350002, China. E-mail: gxu@fjirsm.ac.cn*
[b] *University of Chinese Academy of Sciences, Beijing, 100049, China*
[c] *State Key Laboratory of Photocatalysis on Energy and Environment, Department of Chemistry, Fuzhou University, Fujian, 350002, China*

† Electronic supplementary information (ESI) available: Experimental details, Fig. S1–S17. See DOI: 10.1039/c9cc03443a

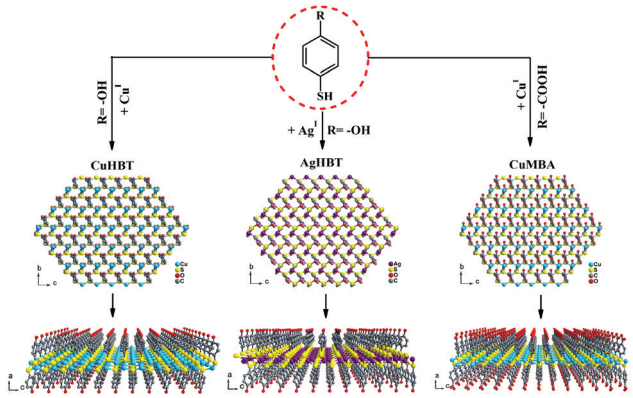

Fig. 1 Schematic representation of the crystal structures of the 2D metal chalcogenide with highly ordered organic functional groups: CuHBT, AgHBT and CuMBA.

CuMBA and AgHBT was 1.45 nm, 1.81 nm and 1.51 nm, respectively (Fig. S1–S3, ESI†).

A representative optical photograph of CuHBT on the Si/SiO_2 substrate indicates the high coverage density of nanosheets (Fig. 2a and Fig. S4, ESI†). Atomic force microscopy (AFM) measurements show that the nanosheets of CuHBT, CuMBA and AgHBT are 4.0–4.5 nm in height and tens of square micrometers in area (Fig. 2b and Fig. S5, ESI†), indicating that the obtained few-layer nanosheets should be 2–3 molecular layers. The powder X-ray diffraction (PXRD) patterns of CuHBT, CuMBA and AgHBT show well-matched diffraction peaks with the simulated ones, suggesting their good crystallinity and high phase purity (Fig. S6 and S7, ESI†). Fig. 2c presents a typical transmission electron microscopy (TEM) image and the corresponding selected area electron diffraction (SAED) pattern of CuHBT. The diffraction in the SAED pattern reveals that the surface of CuHBT is parallel to the (011) plane of the crystal structure, which is the surface that can expose the maximum number of phenol functional motifs (Fig. 2d).

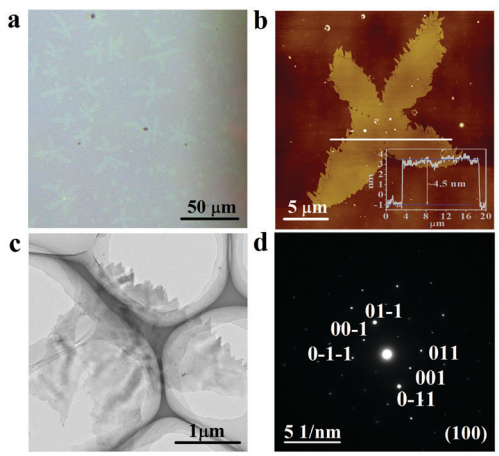

Fig. 2 Morphologies and characterization of CuHBT. (a) Optical photograph of CuHBT on the Si/SiO_2 substrate. (b) AFM image of CuHBT. (c) and (d) TEM image and SAED pattern of CuHBT, respectively.

To investigate its catalytic activity, CuHBT was used as a peroxidase-like catalyst and added to the reaction system containing 3,3′,5,5′-tetramethylbenzidine (TMB) and H_2O_2. The catalytic reaction was detected by monitoring the absorbance increment at 652 nm, which can also be observed to be a blue color by the naked eye. The control experiments without CuHBT showed no color change, indicating that CuHBT is an indispensable catalyst for the reaction (Fig. S8 and S9, ESI†). The time-dependent absorbance changes against the used amount of CuHBT were investigated. The absorbance at 652 nm was gradually saturated when the amount of CuHBT was increased with a maximum level of 35 μg mL^{-1} (Fig. 3a). Furthermore, the above chromogenic reaction is pH dependent. The optimal pH value of the reaction was found to be 4.5 at room temperature (Fig. S10, ESI†), which was determined by comparing the activity related absorbance at 652 nm at different pH. In order to rule out the possibility that the observed activity is caused by the leaching of copper ions or the ligands, 1 μg mL^{-1} CuHBT was incubated in a standard reaction buffer (pH 4.5) for 10 min and then removed from the solution by centrifugation to obtain leaching solution. The leaching solution showed almost no activity when compared with 1 μg mL^{-1} CuHBT (Fig. S11, ESI†). Moreover, it is noticeable that the X-ray photoelectron spectroscopy (XPS) spectra of CuHBT before and after the catalyst reaction are almost the

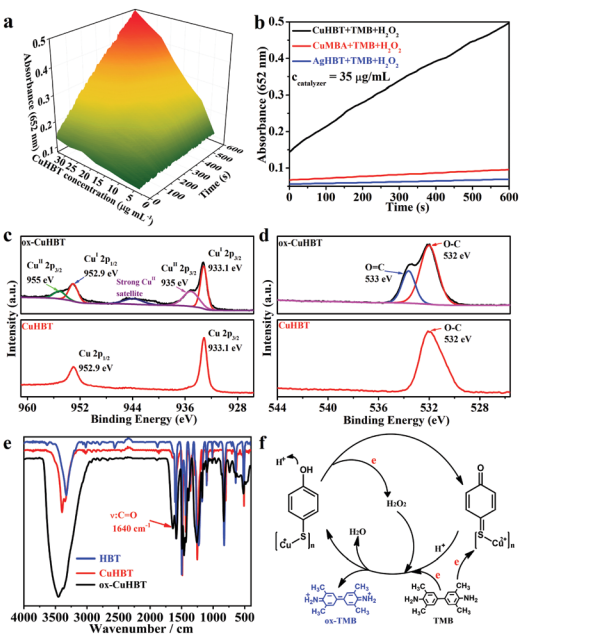

Fig. 3 Mechanistic investigation of the colorimetric reaction of the 2D materials. (a) Time-dependent absorbance changes at 652 nm in various amounts of CuHBT in acetate buffer (100 mM, pH 4.5) containing 8 mM TMB and 0.25 M H_2O_2 at room temperature. (b) Comparison of the time-dependent absorbance changes at 652 nm in the same amount of CuHBT, CuMBA and AgHBT (35 μg mL^{-1}) in acetate buffer (100 mM, pH 4.5) containing 8 mM TMB and 0.25 M H_2O_2 at room temperature. (c and d) XPS data of Cu and O in CuHBT and ox-CuHBT, respectively. (e) IR spectra of the HBT ligand, CuHBT and ox-CuHBT. (f) Schematic representation of the mechanistic investigation of the colorimetric reaction of CuHBT.

same, indicating the high stability of CuHBT as a catalyst (Fig. 3c, d and Fig. S12, ESI†).

To shed more light on the mechanism of the catalytic activity of CuHBT, the same amount of CuMBA and AgHBT was used for comparison. It is found that AgHBT cannot change the color of the reaction solution (Fig. S8, ESI†). Since CuHBT and AgHBT are isostructural with the same ligand, this result suggests that Cu sites play an important role in the catalytic reaction. CuMBA can slightly change the color of the reaction solution (Fig. S8 and S13, ESI†). However, in equal times, the absorbance increment at 652 nm of the CuHBT system is much faster than that of CuMBA (Fig. 3b). These results suggest that Ph–OH in CuHBT is a much better "promoter" than Ph–COOH and can collaborate with Cu sites to synergistically speed up the reaction.

To verify the collaboration of Ph–OH and Cu sites in CuHBT, CuHBT was intentionally reacted with H_2O_2 without TMB. It is found that the color of CuHBT slowly turned to black (denoted as ox-CuHBT) in H_2O_2 (Fig. S14, ESI†). This black color switched back to yellow when CuHBT was put into the TMB solution (Fig. S14, ESI†). The PXRD patterns of CuHBT and ox-CuHBT are almost the same, which reveals that they have the same structure (Fig. S15, ESI†). XPS measurements reveal that only Cu^+ and C–O were found in CuHBT, while discernible concentrations of Cu^{2+} and C═O could be found in ox-CuHBT (Fig. 3c and d). Fourier transform infrared spectroscopy (FTIR) spectra of HBT, CuHBT and ox-CuHBT (Fig. 3e) further confirm the existence of a quinone structure in ox-CuHBT (Fig. S16, ESI†). Compared to the asymmetric vibrations of the benzene ring in CuHBT and HBT, new vibration peaks appearing in the range of 1500–1600 cm^{-1} can be attributed to C═C in ox-CuHBT. The strong vibration peaks for C═S (1256 cm^{-1}) and C═O (1640 cm^{-1}) appear in ox-CuHBT, while the stretching bands of C–S (650 cm^{-1}) and C–O (1253 cm^{-1}) become indistinguishable. These results suggested that quinoid units exist in ox-CuHBT. According to the above observations, the possible role played by CuHBT in catalyzing the reaction between H_2O_2 and TMB was revealed. As shown in Fig. 3f, firstly, the phenol group, as an electron donating group, deprotonates and donates an electron to H_2O_2 to form active species. Meanwhile, Cu^+ donates an electron to the S atom to become Cu^{2+} and the structure of the organic ligand rearranged to form ox-CuHBT. Comparatively, for CuMBA, –COOH is an electron withdrawing group, which makes the conjugated system more electrophilic and relatively difficult to lose electrons to act as a promoter. Next, ox-CuHBT and H_2O_2 active species accept an electron from TMB and a proton from acidic buffer solution, respectively. Ox-CuHBT switches back to CuHBT, H_2O_2 active species become H_2O, while colorless TMB forms blue ox-TMB. The above processes are very similar to the typical ping–pong mechanism found in natural enzyme catalysis reactions, which was further demonstrated by the kinetic analysis of the CuHBT catalysis reaction below.

The apparent steady-state kinetics was investigated using the typical Michaelis–Menten curves, which were obtained for certain concentrations of H_2O_2 or TMB (Fig. S17, ESI†). The apparent K_m value of CuHBT with TMB as the concentration-variable substrate is 0.431 mM, which is similar to those of HRP[11] and GO@Fe_3O_4,[18] and 1.2 times and 4.2 times lower than those of MoS_2[21] and WS_2,[22] respectively. The apparent K_m value of the reaction system with H_2O_2 as the substrate is 0.716 mM, which is 5 times, 215 times and 5.5 times lower than those of HRP,[11] Fe_3O_4 [11] and GO–COOH [17] (Fig. S17, ESI†). These results suggest that CuHBT has good affinity for TMB and H_2O_2, presumably resulting from the strong hydrogen-bond interaction between the substrates and phenol groups which fully cover the surfaces of CuHBT. The double reciprocal plots were characterized with parallel lines, revealing a typical ping–pong mechanism.

Since the catalytic activity of CuHBT is H_2O_2-concentration-dependent, it can be used to detect H_2O_2 (Fig. S17, ESI†). H_2O_2 is one of the main products of the glucose oxidation reaction. Therefore, by coupling the oxidation of glucose catalyzed by glucose oxidase, the chromogenic reaction catalyzed by CuHBT can be further developed into a cascade reaction to quantitatively analyze glucose (Fig. 4a). As shown in Fig. 4b, the intensities of the UV-vis absorption at 652 nm increased upon increasing the concentration of H_2O_2. Fig. 4c presents the H_2O_2 concentration–response curves. The linear response range covered the concentration range of H_2O_2 from 1 to 43 μM, according to the corresponding calibration curve (Fig. 4d), and the limit of detection (LOD) is estimated to be 1 μM. The detection results of glucose are presented in Fig. 4e and f. As illustrated in Fig. 4f, the glucose concentration dependent absorbance at 652 nm was also observed. The absorbance changes at 652 nm can also be verified by the naked eye directly for convenient readout

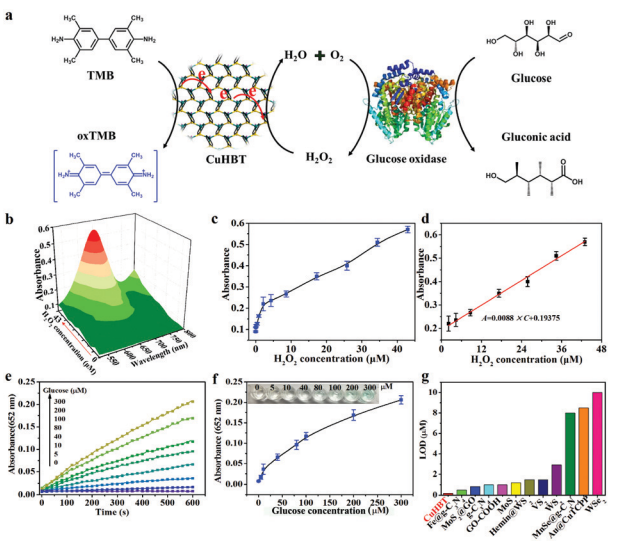

Fig. 4 H_2O_2 and glucose detection by using CuHBT. (a) Schematic illustration of colorimetric detection of glucose catalyzed by using glucose oxidase and CuHBT. (b) Typical UV-vis absorption spectra obtained for detecting H_2O_2 using CuHBT as a peroxidase mimic under the optimized conditions. (c and d) A dose–response curve for H_2O_2 detection using CuHBT. (e) Time-course dependent absorbance changes at 652 nm by increasing the concentration of glucose. (f) A dose–response curve for glucose detection using CuHBT; the inset photograph shows the colored products with different concentrations of glucose (top). (g) Limit of detection of CuHBT compared with other reported 2D materials.

(inset image of Fig. 4f). According to the data, the LOD toward glucose is approximately 0.172 μM. CuHBT shows the lowest detection limit among the reported 2D materials and their composite materials in the one-pot colorimetric detection of glucose (Fig. 4g).[8,17–24]

In conclusion, we have reported a new series of 2D catalytic materials, CuHBT, CuMBA and AgHBT, which possess functional group fully covered surfaces for enhancing their properties as nanozymes. A detailed mechanistic study revealed that the Ph–OH groups on CuHBT surfaces act as ''promoters'' and can significantly enhance the performance of the 2D catalyst. As a result, CuHBT showed excellent intrinsic peroxidase-like catalytic activity and gave rise to the lowest detection limit in the colorimetric detection of glucose among the reported 2D materials and their composite materials. These results suggest full functionalization of the surfaces of 2D materials is an effective way to significantly enhance their performances as nano-biocatalysts.

This work was supported by the National Natural Science Foundation of China (201805276), the Funds for International Cooperation and Exchange of the National Natural Science Foundation of China (21850410462), China Postdoctoral Science Foundation (2018M642576 and 2018M642578), the Natural Science Foundation of Fujian Province (2017J05034), the Youth Innovation Promotion Association CAS and the International Partnership Program of CAS (121835KYSB201800).

Conflicts of interest

There are no conflicts to declare.

Notes and references

1 H. Wei and E. K. Wang, *Chem. Soc. Rev.*, 2013, **42**, 6060.
2 X. Y. Wang, W. J. Guo, Y. H. Hu, J. J. X. Wu and H. Wei, *Nanozymes:next wave of artificial enzymes*, Springer, 2016.
3 Z. C. Sun, J. W. Lv, X. Liu, Z. W. Tang, X. R. Wang, Y. Xu and B. D. Hammock, *Anal. Chem.*, 2018, **90**, 10628.
4 T. Lin, Y. Qin, Y. Huang, R. Yang, L. Hou, F. Ye and S. Zhao, *Chem. Commun.*, 2018, **54**, 1762.
5 X. Niu, X. Xu, X. Li, J. Pan, F. Qiu, H. Zhao and M. Lan, *Chem. Commun.*, 2018, **54**, 13443.
6 Q. Chen, M. Liu, J. Zhao, X. Peng, X. Chen, N. Mi, B. Yin, H. Li, Y. Zhang and S. Yao, *Chem. Commun.*, 2014, **50**, 6771.
7 J. Mu, Y. Wang, M. Zhao and L. Zhang, *Chem. Commun.*, 2012, **48**, 2540.
8 Y. Huang, M. Zhao, S. Han, Z. Lai, J. Yang, C. Tan, Q. Ma, Q. Lu, J. Chen, X. Zhang, Z. Zhang, B. Li, B. Chen, Y. Zong and H. Zhang, *Adv. Mater.*, 2017, **29**, 1700102.
9 Y. Jv, B. Li and R. Cao, *Chem. Commun.*, 2010, **46**, 8017.
10 W. Shi, Q. Wang, Y. Long, Z. Cheng, S. Chen, H. Zheng and Y. Huang, *Chem. Commun.*, 2011, **47**, 6695.
11 L. Gao, J. Zhuang, L. Nie, J. Zhang, Y. Zhang, N. Gu, T. Wang, J. Feng, D. Yang, S. Perrett and X. Yan, *Nat. Nanotechnol.*, 2007, **2**, 577.
12 Y. Chen, T. Hoang and S. Ma, *Inorg. Chem.*, 2012, **51**, 12600.
13 D. Feng, Z. Gu, J. Li, H. Jiang, Z. Wei and H. Zhou, *Angew. Chem., Int. Ed.*, 2012, **51**, 10307.
14 L. Ai, L. Li, C. Zhang, J. Fu and J. Jiang, *Chem. – Eur. J.*, 2013, **19**, 15105.
15 J. Zhang, H. Zhang, Z. Du, X. Wang, S. Yu and H. L. Jiang, *Chem. Commun.*, 2014, **50**, 1092.
16 C. Tan, X. Cao, X. Wu, Q. He, J. Yang, X. Zhang, J. Chen, W. Zhao, S. Han, G.-H. Nam, M. Sindoro and H. Zhang, *Chem. Rev.*, 2017, **117**, 6225.
17 Y. Song, K. Qu, C. Zhao, J. Ren and X. Qu, *Adv. Mater.*, 2010, **22**, 2206.
18 Y. Dong, H. Zhang, Z. U. Rahman, L. Su, X. Chen, J. Hu and X. Chen, *Nanoscale*, 2012, **4**, 3969.
19 J. Tian, Q. Liu, A. M. Asiri, A. H. Qusti, A. O. Al-Youbi and X. Sun, *Nanoscale*, 2013, **5**, 11604.
20 T. Lin, L. Zhong, J. Wang, L. Guo, H. Wu, Q. Guo, F. Fu and G. Chen, *Biosens. Bioelectron.*, 2014, **59**, 89.
21 T. Lin, L. Zhong, L. Guo, F. Fu and G. Chen, *Nanoscale*, 2014, **6**, 11856.
22 T. Lin, L. Zhong, Z. Song, L. Guo, H. Wu, Q. Guo, Y. Chen, F. Fu and G. Chen, *Biosens. Bioelectron.*, 2014, **62**, 302.
23 J. Peng and J. Weng, *Biosens. Bioelectron.*, 2017, **89**, 652.
24 T. Chen, X. Wu, J. Wang and G. Yang, *Nanoscale*, 2017, **9**, 11806.
25 J. Benck, T. Hellstern, J. Kibsgaard, P. Chakthranont and T. Jaramillo, *ACS Catal.*, 2014, **4**, 3957.
26 J. Kibsgaard, Z. Chen, B. Reinecke and T. Jaramillo, *Nat. Mater.*, 2012, **11**, 963.
27 L. Yang, H. Hong, Q. Fu, Y. Huang, J. Zhang, X. Cui, Z. Fan, K. Liu and B. Xiang, *ACS Nano*, 2015, **9**, 6478.
28 D. Chung, S. Park, Y. Chung, S. Yu, D. Lim, N. Jung, H. Ham, H. Park, Y. Piao, S. Yoo and Y. Sung, *Nanoscale*, 2014, **6**, 2131.
29 J. Lauritsen, J. Kibsgaard, S. Helveg, H. Topsøe, B. Clausen, E. Lægsgaard and F. Besenbacher, *Nat. Nanotechnol.*, 2007, **2**, 53.
30 Y. Zhang, Q. Ji, G. Han, J. Ju, J. Shi, D. Ma, J. Sun, Y. Zhang, M. Li, X. Lang, Y. Zhang and Z. Liu, *ACS Nano*, 2014, **8**, 8617.
31 K. Low, V. Roy, S. Chui, S. Chana and C. Che, *Chem. Commun.*, 2010, **46**, 7328.
32 J. Troyano, O. Castillo, J. I. Martínez, V. Fernández-Moreira, Y. Ballesteros, D. Maspoch, F. Zamora and S. Delgado, *Adv. Funct. Mater.*, 2018, 1704040.
33 I. G. Dance, K. J. Fisher, R. M. H. Banda and M. L. Scudder, *Inorg. Chem.*, 1991, **30**, 183.